HHS Public Access

Author manuscript

J Immunol. Author manuscript; available in PMC 2017 September 01.

Published in final edited form as:

J Immunol. 2016 September 1; 197(5): 1823–1831. doi:10.4049/jimmunol.1600717.

Leishmania major infection-induced VEGF-A/VEGFR-2 signaling promotes lymphangiogenesis that controls disease[1]

Tiffany Weinkopff[*], **Christoph Konradt**[*], **David A. Christian**[*], **Dennis E. Discher**[†], **Christopher A. Hunter**[*], and **Phillip Scott**[*,‡,1]

[*]Department of Pathobiology, School of Veterinary Medicine, University of Pennsylvania, Philadelphia, PA, 19104, USA

[†]Biophysical Eng'g Labs, University of Pennsylvania, Philadelphia, PA, 19104, USA

Abstract

Cutaneous leishmaniasis causes a spectrum of diseases from self-healing to severe non-healing lesions. Defining the factors contributing to lesion resolution may help in developing new therapies for those patients with chronic disease. We found that infection with *Leishmania major* increases the expression of vascular endothelial growth factor-A (VEGF-A) and vascular endothelial growth factor receptor-2 (VEGFR-2), and is associated with significant changes in the blood and lymphatic vasculature at the site of infection. Antibody blockade of VEGFR-2 during infection led to a reduction in lymphatic endothelial cell proliferation and simultaneously increased lesion size without altering the parasite burden. These data show that *L. major* infection initiates enhanced VEGF-A/VEGFR-2 signaling, and suggest that VEGFR-2-dependent lymphangiogenesis is a mechanism that restricts tissue inflammation in leishmaniasis.

INTRODUCTION

Cutaneous leishmaniasis has a wide spectrum of clinical manifestations, ranging from self-healing to chronic debilitating disease. Presently, there is no vaccine for human leishmaniasis, the drugs against the parasite are extremely toxic, and furthermore patients are often refractory to treatment (1-3). *Leishmania* parasites are killed by macrophages in response to IFNγ produced by $CD4^+$ Th1 cells, and thus severe disease occurs in the absence of a strong Th1 response (4). However, even when an appropriate adaptive immune response develops and parasites are controlled, cutaneous lesions often persist suggesting the inflammatory response can drive pathology (5-8). Thus, defining the factors that control both lesion development and resolution is important in developing novel therapies to address the disease in patients.

While many factors have been shown to contribute to the development and severity of leishmanial lesions (5, 7-9), the role of changes in the vasculature in cutaneous leishmaniasis

[‡]Corresponding author: Phillip Scott, Department of Pathobiology, School of Veterinary Medicine, 380 South University Ave., Philadelphia, PA 19104-4539, Phone: 215-898-1602, Fax: 215-746-2294, pscott@vet.upenn.edu.

[1]Imaging experiments were carried out on instrumentation supported by NIH S10RR027128, the School of Veterinary Medicine, the University of Pennsylvania, and the Commonwealth of Pennsylvania. T.W. was supported by the NIH postdoctoral research grant F32 AI 114080. This work was supported by NIH grants (R01 AI 106842 to P.S. and R01 AI 41158 to C.A.H.).

has not been explored. Vascular remodeling is a hallmark of inflammation and leads to morphological and functional changes of the vascular network that can influence both the recruitment of cells as well as their exit from the tissue (10-13). The formation of new blood vessels during inflammation and the increased vascular permeability enhances cell recruitment, but concomitantly may also promote pathology (10-14). Moreover, the expansion of the lymphatic vasculature which supports the initial immune response, also provides a route for drainage of fluid and inflammatory cells out of the tissue (10, 15, 16).

Members of the vascular endothelial growth factor family including VEGF-A, VEGF-C and VEGF-D are produced by a variety of cell types and induce changes in the vascular network during cancer, wound healing and inflammation. VEGF-A binds VEGFR-2, which is primarily expressed on blood ECs, and promotes angiogenesis and vascular permeability (17). Alternatively, VEGF-C and VEGF-D bind to VEGFR-3 on lymphatic ECs promoting lymphangiogenesis (18). VEGF family members are elevated in inflammatory settings, and neutralization of VEGFR-2 signaling reduces inflammation, while VEGFR-3 blockade increases inflammation in the skin (15, 19). Even though VEGF-A binding VEGFR-2 on blood ECs primarily leads to angiogenesis, VEGF-A can also mediate inflammation-induced lymphangiogenesis, and VEGF-A produced in the skin can have profound effects at other sites, such as the draining lymph node (dLN) (20-24). Thus, VEGF signaling might be important in the development and resolution of leishamanial lesions, and currently the role of this pathway has not been defined during infection.

To address this question, we examined the role of VEGF signaling in cutaneous leishmaniasis. Here, we show that *L. major* infection induces vascular remodeling in the skin and that the expression of VEGF-A and its receptor VEGFR-2 are elevated. The kinetics of the expression of these mediators mirrors the presence of leishmanial lesions and coincides with increased blood and lymphatic endothelial cell (EC) proliferation at the infection site. Moreover, inhibition of VEGF-A/VEGFR-2 signaling during *L. major* infection specifically affected lymphatic ECs and led to increased disease pathology. Taken together, these data suggest that *L. major* infection activates the VEGF-A/VEGFR-2- signaling pathway leading to vascular remodeling, and suggests that VEGFR-2-mediated lymphangiogenesis is a mechanism that limits inflammation and promotes lesion resolution.

MATERIALS AND METHODS

Mice

Female C57BL/6 mice were purchased from the National Cancer Institute and Tie2-GFP transgenic mice, where GFP is predominantly expressed by ECs, were purchased from Jackson Laboratories and bred at the University of Pennsylvania. Mice were housed in the School of Veterinary Medicine at the University of Pennsylvania under pathogen-free conditions and used for experiments between 6-8 weeks of age. All procedures were performed in accordance with the guidelines of the University of Pennsylvania Institutional Animal Care and Use Committee.

Parasites and Infections

The *Leishmania major* (WHO/MHOM/IL/80/Friedlin) strain was used for experiments. Parasites were grown *in vitro* in Schneider's Drosphilia medium (GIBCO) supplemented with 20% heat-inactivated fetal bovine serum (FBS, Invitrogen), 2 mM L-glutamine (Sigma) and 2 mM L-glutamine (Sigma), 100 U/mL penicillin and 100 μg/mL streptomycin (Sigma). Metacyclic stationary phase promastigotes were isolated from 4-5 day cultures by Ficoll density gradient separation (Sigma) (25). For dermal ear infections, 2×10^6 parasites in 10 μL PBS (Lonza) were injected intradermally into the ear. Lesion development was monitored weekly by measuring ear thickness and lesion area with a caliper and the lesion volume was calculated. Pathology was also scored using the previously published scoring system: no lesion (0), swelling/redness (1), deformation of the ear pinna (2), ulceration (3), partial tissue loss (4), or total tissue loss (5) (26). To determine parasite loads and cellular content, ears were enzymatically digested using 0.25 mg/mL liberase (Roche) and 10 μg/mL DNAse I (Sigma) in incomplete RPMI (GIBCO) for 90 min at 37 C. To determine parasite burdens in the tissue, limiting dilution assays were performed (27).

Histology and Immunofluorescence Microscopy

For histology, *L. major* infected and naïve ears were fixed in 10% buffered formalin and embedded in paraffin. Longitudinal 6 μm sections were subjected to Masson's trichrome stain. For immunofluorescence microscopy, ears and dLNs were frozen in Tissue-Tek OCT (Sakura). Longitudinal 6 μm sections were fixed with 3% formaldehyde, blocked with 10% goat serum (Sigma) for 1 h and stained with rat α-CD31 (BD Pharmingen) and rabbit α-LYVE-1 (AngioBio Co.) overnight followed by secondary antibodies goat α-rabbit AF488 (Life Technologies) or goat α-rat DyLight 549 (Jackson ImmunoResearch) for 1 h. Sections were stained with DAPI (Molecular Probes) and mounted with Prolong Gold (Life Technologies). Images were captured using a Nikon Digital Sight DS-Fi1 color camera on a Nikon E600 microscope.

Multiphoton Microscopy

Mice were anaesthetized and maintained at core temperature of 37 °C. Ears were attached to an imaging platform using tissue glue. The mice were injected retrorbitally with 50 μL of 1% Evans blue (Alfa Aesar) and imaged immediately. Imaging was performed with a Leica SP5 2-photon microscope system (Leica Microsystems) equipped with a picosecond or femtosecond laser (Coherent). The standard wavelength used for the two-photon imaging was 900 nm, which allowed optimal excitation of the used fluorophores. Images were obtained using a 20x water-dipping lens. The total volume of the fluorescence of Evans blue was calculated using Volocity (Perkin Elmer) at time point zero (approximately 2 min after injection), and the calculated fluorescence at time point zero was subtracted from subsequent time points.

Vascular Leakage

Near infrared nano-polymersomes were formed by first dissolving an amphiphilic diblock copolymer composed of polyethylene glycol and polybutadiene (PEG-PBD) in chloroform with the lipophilic near IR (NIR) fluorophore DiR (ThermoFisher Scientific). This solution

was then evaporated to form a thin polymer film, and polymersomes were formed by film rehydration at 60 °C overnight. Nano-polymersomes were then synthesized by sonication and extrusion to an average diameter of 200 nm as previously described (28). Mice were injected i.v. with NIR nano-polymersomes and the accumulation of NIR fluorescence was imaged from whole mount tissues of infected and contralateral ears after 3 h using an Odyssey infrared imaging system (LI-COR Biosciences). For the Miles assay, 100 μL 4% Evans blue was injected i.v. and ears were weighed and imaged after 2 h. The dye was extracted from the tissue by placing ears in formamide for 48 h at 60 °C. The samples were centrifuged and the optical density at 650 nm was recorded. The amount of Evans blue per ear was calculated using a standard curve and the weight of the tissue.

Flow Cytometry

Cells were incubated with fixable Aqua dye (Invitrogen) to assess viability. FcRs were blocked with CD16/32 (eBioscience, San Diego, CA) and cells were surface stained using α-CD45, α-Ly6C, and α-VEGFR-2 (from eBioscience), as well as α-CD64, α-CD11b, α-CD31 and α-podoplanin-biotin (from BioLegend), followed by streptavidin-PECy7 (eBioscience). For intracellular cytokine staining, dLN cells were stimulated with Brefeldin A (BFA, 3 μg/mL, eBiosciences) with phorbol myristate acetate (PMA, 100 ng/mL, Sigma) and ionomycin (1 μg/mL, Sigma) for 4 hours before surface staining for α-CD4. dLN cells were then fixed with 2% paraformaldehyde (Electron Microscopy Sciences), permeabilized with 0.2% saponin buffer and stained for α-IFNγ (BioLegend). Cell events were acquired on LSRII Fortessa flow cytometer (BD Biosciences, San Jose, CA) and analyzed using FlowJo (Tree Star).

BrdU Incorporation

BrdU (BD Pharmingen) was placed in the drinking water (0.8 mg/mL) for three days and mice were injected i.p. with 1 mg of BrdU 24 h and 1 h prior to euthanasia. After tissue processing and cell surface staining, cells were fixed and permeabilized the BrdU kit (BD Pharmingen) and intracellularly stained with α-BrdU-APC after DNAse I treatment according the manufacturer's instructions.

Quantitative Real-time PCR

mRNA was extracted by the RNeasy Plus Mini kit (Qiagen). RNA was reverse transcribed with high capacity cDNA Reverse Transcription (Applied Biosystems). Quantitative real-time PCR was performed using SYBR Green PCR Master Mix on a ViiA 7 real-time PCR system (Life Technologies). Primer sequences are listed in Table S1. The results were normalized to the housekeeping gene ribosomal protein S14 gene (RPSII) using the comparative threshold cycle method ($2^{-\Delta\Delta CT}$) for relative quantification (8, 29).

VEGFR-2 Inhibition in vivo

Mice were given α-VEGFR-2 DC101 antibody (0.8 mg/mouse i.p. every 3 days) kindly provided by Bronislaw Pytowski at Eli Lilly and Company (New York, NY) or rat IgG control (clone 2A3; BioXCell) starting one day prior to infection continuing for the first 4 weeks of infection.

Statistics

Statistical significance was determined using a two-tailed Student's unpaired *t*-test with a p value < 0.05 in GraphPad Prism 5.

RESULTS

Dermal vascular remodeling occurs during *L. major* infection

Given that human leishmanial lesions exhibit VEGF-A and VEGFR-2 expression and VEGF-A/VEGFR-2 signaling can contribute to the inflammatory response through remodeling of the vasculature, the role of vascular remodeling was evaluated in cutaneous leishmaniasis. Cutaneous leishmaniasis was studied using the well-characterized experimental murine model where C57BL/6 mice were dermally infected with *L. major* parasites. In this model, dermal lesions slowly develop, peaking at 4-6 weeks p.i. with 10^6-10^7 parasites in the lesions. Once parasites are controlled by the immune response, dermal lesions in C57BL/6 mice spontaneously resolve by 8-10 weeks p.i. (Fig. 1A). In order to visualize the ECs and vasculature following infection Tie2-GFP reporter mice. Mice were infected with *L. major* parasites in the ear and the vasculature was analyzed using multiphoton intravital microscopy (30). Compared to naïve mice, at 5 weeks p.i. when lesions are at their peak, the structure and morphology of the vessels in infected skin is highly tortuous and irregularly shaped with sprouts, reminiscent of tumor vessels (Fig. 1B and 1F). Histology of infected ears also revealed an increase in the number of vessels in the skin over time that mirror lesion development (Fig. 1C-D). In addition, immunofluorescence microscopy showed an increase in CD31 staining, a marker of ECs, in the ears of infected mice compared to controls (Fig. 1E). Taken together, these data show that *L. major* infection induces vascular remodeling in the skin, and increases in $CD31^+$ cells suggests an expansion of the EC network.

Endothelial cell proliferation is detected at the site of infection during leishmaniasis

Vascular remodeling is often associated with the proliferation of ECs. Therefore, the frequency of proliferating ECs during *L. major* infection was examined by BrdU incorporation in C57BL/6 mice. At 20 days p.i., when lesions are starting to develop in infected mice, flow cytometric analysis of $CD45^-$ $CD31^+$ ECs revealed an increase in the percentage and number of $BrdU^+$ proliferating ECs compared to naïve control skin (Fig. 2A-C). The percentage of $BrdU^+$ proliferating ECs was elevated as early as 12 days p.i. when lesions are not yet apparent in infected mice, and increased percentages of $BrdU^+$ ECs persist in infected ears at day 35 p.i. when lesions are at their peak (Fig. 2B). Blood and lymphatic ECs can be distinguished based on their podoplanin expression as blood ECs (BECs) are $CD31^+$ $podoplanin^-$ and lymphatic ECs (LECs) are $CD31^+$ $podoplanin^+$ (Fig. 2D). When BEC and LEC populations were examined individually, flow cytometric analysis showed increased percentages and numbers of $BrdU^+$ BECs in infected mice compared to naïve controls (Fig. 2E-G). Similarly, *L. major*-infected ears displayed increased percentages and numbers of $BrdU^+$ LECs compared to controls (Fig. 2E and 2H-I). Altogether, these results clearly indicate that EC proliferation is ongoing at the site of infection and suggests *L. major* infection triggers angiogenesis and lymphangiogenesis in the dermis, and this rapid

expansion of the blood and lymphatic vasculature likely has a strong effect on vessel permeability within the infected tissue.

Increased vascular permeability in the dermis is associated with *L. major* infection

Vascular remodeling often coincides with enhanced vascular permeability, which allows cells and inflammatory mediators to migrate into inflamed tissues. To determine if *L. major* infection leads to increased vascular permeability in the skin, C57BL/6 were infected in the ear and at 5 weeks p.i. mice were injected i.v. with nano-polymersomes containing a near-infrared fluorophore 3 h prior to ex vivo imaging of whole mount ear tissue. The size of the nano-polymersomes (average diameter of 200 nm) prevents these particles from escaping through normal vasculature but have been shown to accumulate at sites of enhanced permeability (31). Imaging showed infected ears with an increase in fluorescence compared to controls, suggesting that more polymersomes accumulated in the infected ear compared to the contralateral ear of the same mouse (Fig. 3A-B). Moreover, the polymersomes specifically collected at lesions within the infected ears, suggesting increased vascular leakage directly at the infection site. In complementary experiments, C57BL/6 mice were subjected to a Miles assay at 5 weeks p.i. in which Evans blue was injected intravenously (32). Infected ears had a greater amount of Evans blue collect in the tissue compared to contralateral ears (Fig. 3C-D). To examine the extent and proximity of vascular leakage with parasitized cells, intravital multiphoton imaging was used to visualize cutaneous vascular leakage in real time after infection with DsRed-labeled parasites. For these experiments, naïve and infected Tie2-GFP mice were given Evans blue i.v. and imaged immediately. Images of the ear were acquired every 30 sec for 30 min. Time-lapsed images revealed that the Evans blue stayed confined within the vasculature in naïve control ears (Fig. 3E-G and Movies 1 and 3). In contrast, the Evans blue escaped out of the vessels and into the extravascular space in infected ears (Fig. 3E-G and Movies 2 and 4). Collectively, these data demonstrate *L. major* infection induces dramatic changes in the cutaneous vasculature, including an increase in vascular permeability.

VEGF-A and VEGFR-2 are expressed at increased levels at the site of *L. major* infection

Given that VEGFs are the primary vascular mediators responsible for EC proliferation and increased vascular permeability, the kinetics of the expression of multiple VEGF family members during *L. major* infection in vivo were examined. At 5 weeks p.i., the expression of VEGF-A (Fig. 4A) and its receptor VEGFR-2 (Fig. 4B) were elevated at the site of infection in C57BL/6 mice compared to naïve skin. VEGF-C, VEGF-D and their receptor VEGFR-3 were not significantly elevated at the time points analyzed (Fig. 4C-E). The kinetics of VEGF-A expression mirrors the development and resolution of leishmanial lesions and coincides with increased EC proliferation. Since VEGF-A transcript levels were elevated in the skin at the site of infection, the expression of VEGF-A was also examined in the dLN. Similar to the site of infection, the expression of VEGF-A was significantly increased in the LN draining infected ears compared to naïve controls (Fig. 4F). Transcript levels of HIF1α, which drives VEGF-A expression, were shown to be increased in both the ear and dLN at 5 weeks p.i., compared to naïve controls (Fig. 4G-H). Taken together these data show that the angiogenic HIF1α/VEGF-A/VEGFR-2 pathway is elevated during leishmaniasis and may play a role in vascular remodeling at the site of infection.

Inhibition of VEGF-A/VEGFR-2 signaling targets lymphangiogenesis and increases pathology during leishmaniasis

Since vascular remodeling, including increased EC proliferation and vascular leakiness, was associated with elevated VEGF-A and VEGFR-2 levels during *L. major* infection, the role of the VEGF-A/VEGFR-2 pathway was analyzed in vivo using an antibody neutralization strategy. Inhibition of VEGFR-2 signaling from the onset of infection reduced $CD31^+$ EC proliferation as assessed by BrdU incorporation at 2 weeks p.i. (Fig. 5A-B). Additionally, the BECs and LECs were analyzed individually based on their podoplanin expression and VEGFR-2 blockade led to a decrease in the percentage of $BrdU^+$ LECs during infection (Fig. 5A and 5D). However, surprisingly the frequency of $BrdU^+$ BECs was not altered with VEGFR-2 blockade suggesting VEGFR-2 inhibition specifically limited the proliferation of LECs without affecting BEC proliferation at the site of infection (Fig. 5A and 5C-D). Given that inhibition of VEGFR-2 signaling targeted LECs and not BECs, we next compared the expression of VEGFR-2 on dermal BECs and LECs. Flow cytometric results showed LECs expressed higher levels of VEGFR-2 than BECs in the skin of both naïve and infected mice supporting the preferential effects seen in LECs with antibody blockade (Fig. 5E). To determine if VEGFR-2 blockade altered parasite control or disease pathology, C57BL/6 mice were infected and given αVEGFR-2 antibody for the first 4 weeks of infection. Importantly, mice receiving αVEGFR-2 antibody exhibited increased lesion volumes compared to isotype control treated mice (Fig. 5F). Additionally, inhibition of VEGFR-2 signaling exacerbated pathology and some mice developed ulcerations, which was rarely seen in the control group (Fig. 5G-H). These increased lesion sizes were not associated with impaired parasite control as parasite burdens in mice treated with αVEGFR-2 antibody were not higher at 4 weeks p.i. compared to controls (Fig. 5I). Additionally, there were no significant differences in the percentages of immune cell populations including macrophages, $Ly6C^+$ inflammatory monocytes, or $CD4^+$ T cells in the dermis of mice treated with αVEGFR-2 antibody compared to controls at 4 weeks p.i. (Fig. 5J). Furthermore, the frequency of $CD4^+$ T cells producing IFNγ in the dLN was similar between groups (Fig. 5J). Similarly, the transcript levels of IFNγ, IL-4 or IL-10 at the site of infection did not differ between mice treated with αVEGFR-2 antibody compared to controls (data not shown). Given T regulatory cells (Tregs) and plasmacytoid dendritic cells (pDCs) are known to express VEGFR2, the frequency of these immune cell populations was also examined following infection; however, the percentage of Tregs and pDCs was similar with and without VEGFR-2 blockade following infection (data not shown). Histologically, ears from mice given αVEGFR-2 antibody showed a cellular infiltrate that exceeded control animals (Fig. 5K). Additionally, ears were stained with LYVE-1 to examine the lymphatic vasculature by immunofluorescence. VEGFR-2 blockade led to decrease in lymphatic vessel diameter compared to isotype-treated controls, but did not alter density of lymphatic vessels at the site of infection (Fig. 5L-N). Taken together these data suggest VEGF-A/VEGFR-2 signaling mediates the proliferation of LECs and contributes to lymphangiogenesis during infection, and that inhibition of this pathway exacerbates pathology demonstrating a protective role for the VEGF-A/VEGFR-2 signaling pathway during infection-induced inflammation.

DISCUSSION

While the immune response to *L. major* has been well characterized, changes in the vasculature that might influence disease progression have not been investigated. Thus, many studies have focused on the frequency and activation status of immune cells at the site of infection, but little work has gone into understanding how the vasculature contributes to the immune response during infection, or if manipulation of the pathways involved in vascular remodeling alters pathogen control, pathology and/or lesion resolution. Here, we have shown *L. major* infection leads to dramatic morphological changes in the dermal vascular network. The vessels from infected mice were found to be highly tortuous and dilated, reminiscent of the vasculature associated with tumors, and exhibited increased permeability, confirming recent findings in this model (33). Infection also increased EC proliferation and the levels of VEGF-A and VEGFR-2. These findings are relevant to human leishmaniasis, as VEGF-A and VEGFR-2 are expressed in leishmanial lesions from humans along with dilated vessels, corroborating our findings in the mouse model (34). To determine if VEGF-A/VEGFR-2 signaling contributes to pathogen control or the severity of disease, infected mice were given VEGFR-2 blocking antibodies, which specifically decreased the percentage of proliferating LECs and exacerbated pathology. These data suggest VEGF-A/VEGFR-2 signaling mediates vascular remodeling and contributes to infection-induced lymphangiogenesis that serves as a protective mechanism to restrict the inflammatory response.

During *L. major* infection we found elevated levels HIF1α, which is the major transcription factor that responds to oxygen deprivation and cellular stress. HIF activation can occur in response to hypoxia, cytokines, TLR ligation, and ROS, all of which are present during *L. major* infection. Thus, we hypothesize HIF1α activation is driving VEGF-A expression and production during infection. Parasites may directly activate HIF1α themselves or the hypoxic environment rich in proinflammatory cytokines such as TNFα and IL-1 may also contribute to HIF activation and thus VEGF-A production (35-37). Furthermore, *Leishmania spp*. can activate TLRs, so VEGF-A production may result from HIF1α activation in response to TLR ligation (29, 38-40). Additionally, *Leishmania spp*. can induce ROS from monocytes and macrophages, so ROS may activate HIF1α and thus VEGF-A production during infection (41). As a result, ongoing work in the lab is focused on dissecting out the individual roles of host and parasite factors that may act alone or in a combinatorial fashion to enhance HIF activation and thus VEGF-A expression and production following *L. major* infection.

At present, the cellular source of VEGF-A has not been identified, and it remains to be determined if VEGF-A expression is directly mediated by HIF1α during leishmaniasis. Given their role in other inflammatory settings and cancer, we hypothesize that myeloid cells, which are present at high numbers in leishmanial lesions, are responding to factors in the tissue driving HIF1α activation and thus VEGF-A expression and production (20, 22, 42, 43). Therefore, we speculate myeloid cells are the major producers of VEGF-A in vivo following *L. major* infection. However, other cells such as keratinocytes, DCs, and B cells can contribute to VEGF-A production in wound healing and inflammation and may play a role in this setting (21, 44). Therefore, future studies aim to identify the cellular source of

VEGF-A, and to determine if VEGF-A production is mediated by HIF1α activation following *L. major* infection. During infection, we hypothesize that myeloid cells located at the lesion site produce VEGF-A that predominantly targets LECs in the skin to initiate lymphangiogenesis. We speculate that ECs are the primary targets of VEGF-A given their high expression levels of VEGFR-2, but other cells types such as macrophages also express VEGFR-2 suggesting VEGF-A may also be acting on hematopoietic cells during infection. As a result, future studies will characterize the effects of VEGF-A on immune cell populations during *L. major* infection.

During *L. major* infection, VEGFR-2 signaling limits pathology by increasing lymphatic vessel number and function. Surprisingly, we found that VEGFR-2 signaling induces LEC proliferation and lymphangiogenesis following *L. major* infection. This result was unexpected given VEGFR-2 signaling is typically thought to mediate angiogenesis and promote dermal pathology (19). Although less appreciated, VEGF-A can drive lymphangiogenesis but lymphangiogenesis is primarily mediated by VEGF-C/-D/VEGFR-3 signaling (19, 22, 24, 45-47). In addition to decreased lymphangiogenesis, lymphatic vessel diameter was decreased with VEGFR-2 blockade, similar to results obtained using skin UVB-irradiation (48). These findings suggest collapsed lymphatic vessels may be functionally impaired in their ability to transport fluid and cells away from the site of inflammation. Even though VEGFR-2 blockade resulted in larger leishmanial lesions, these mice controlled parasites similar to controls, which is consistent with a lack of differences in the immune response between groups (data not shown). These data suggest the preexisting lymphatic vasculature is sufficient to drive the adaptive immune response, but VEGFR-2-mediated lymphangiogenesis is required to drain fluid and newly infiltrated cells away from the site of infection. Moreover, lymphangiogenesis is also required for normal wound repair and the increased pathology during *L. major* infection may reflect a defect in lesion resolution (42, 46, 49). Altogether, our studies show *L. major* infection induces VEGF-A/VEGFR-2 signaling that promotes lymphangiogenesis and protects against exacerbating pathology.

Our data suggests VEGF-A/VEGFR-2 signaling is not essential for angiogenesis during *L. major* infection so other factors such as FGF-2, PDGF, and angiopoietins may contribute to angiogenesis. Importantly, these pathways can induce angiogenesis in the absence of VEGFR-2 signaling (50-56). Therefore, we hypothesize that other angiogenic mediators, such as FGF-2 that is elevated during infection, may drive the expansion of the blood vasculature during leishmaniasis (57). Alternatively, these angiogenic factors may serve a redundant or compensatory role only upon the neutralization of VEGFR-2.

In this study, *L. major* infection led to elevated levels of VEGF-A and increased EC proliferation in both the dermis and the dLN. However, VEGFR-2 blockade led to a reduction in EC proliferation in the ear while no differences were detected in the dLNs. Consistent with this observation, the size and cellularity of the dLNs was similar between mice treated with αVEGFR-2 antibody and controls. In the dLN, the VEGFR-2 and VEGFR-3 pathways may compensate for one another for EC proliferation. Alternatively, other signaling pathways, such as the lymphotoxin β/LTβR or LIGHT/LTβR, which have been shown to be important in both dLN hypertrophy as well as *L. major* infection, may also

contribute to EC proliferation (58-61). Furthermore, the lack of inhibition of EC proliferation in the total dLN may not reflect differences in distinct regions of the dLN (62). In addition, we found higher expression levels of VEGFR-2 in the dermis compared to the dLN so blockade strategies may preferentially affect cells in the skin. As a result, studies are ongoing in the lab to identify the pathways responsible for angiogenesis and lymphangiogenesis in the dLN during infection.

In summary, we have shown that *L. major* infection activates VEGF-A/VEGFR-2 signaling which promotes vascular remodeling and drives the expansion of the lymphatic network providing a conduit for fluid and cells to migrate to the dLN. Upon blockade of VEGFR-2-mediated lymphangiogenesis, we speculate that fluid, debris and cells are sequestered at the site of infection resulting in exacerbated pathology. Since the lesions of many patients with leishmaniasis exhibit an immense inflammatory infiltrate, despite low numbers of parasites, stimulation of lymphangiogenesis may provide a novel target to alleviate the inflammation. Thus, understanding the role of the vasculature during infection and inflammation has important implications for development of novel strategies targeting the vasculature to limit the pathology associated with parasites as well as other infectious and inflammatory diseases.

Supplementary Material

Refer to Web version on PubMed Central for supplementary material.

ACKNOWLEDGMENTS

The authors would like to thank Drs. Gudrun Debes, Sydney Evans, and Celeste Simon for their discussion and Ba Nguyen for technical assistance (University of Pennsylvania). We acknowledge the Abramson Cancer Center Histology Core and the Flow Cytometry Core Facility in the School of Medicine as well as the PennVet Imaging Core Facility and specifically Dr. Gordon Ruthel at the University of Pennsylvania.

REFERENCES

1. Koff AB, Rosen T. Treatment of cutaneous leishmaniasis. J. Am. Acad. Dermatol. 1994; 31:693–708. quiz 708-610. [PubMed: 7523464]
2. Kumar R, Engwerda C. Vaccines to prevent leishmaniasis. Clin. Transl. Immunology. 2014; 3:e13. [PubMed: 25505961]
3. Tiuman TS, Santos AO, Ueda-Nakamura T, Filho BP, Nakamura CV. Recent advances in leishmaniasis treatment. Int. J. Infect. Dis. 2011; 15:e525–532. [PubMed: 21605997]
4. Kaye P, Scott P. Leishmaniasis: complexity at the host-pathogen interface. Nat. Rev. Microbiol. 2011; 9:604–615. [PubMed: 21747391]
5. Bacellar O, Lessa H, Schriefer A, Machado P, Ribeiro de Jesus A, Dutra WO, Gollob KJ, Carvalho EM. Up-regulation of Th1-type responses in mucosal leishmaniasis patients. Infect. Immun. 2002; 70:6734–6740. [PubMed: 12438348]
6. Bittencourt AL, Barral A. Evaluation of the histopathological classifications of American cutaneous and mucocutaneous leishmaniasis. Mem. Inst. Oswaldo Cruz. 1991; 86:51–56. [PubMed: 1842401]
7. Terabe M, Kuramochi T, Ito M, Hatabu T, Sanjoba C, Chang KP, Onodera T, Matsumoto Y. CD4(+) cells are indispensable for ulcer development in murine cutaneous leishmaniasis. Infect. Immun. 2000; 68:4574–4577. [PubMed: 10899857]
8. Gonzalez-Lombana C, Gimblet C, Bacellar O, Oliveira WW, Passos S, Carvalho LP, Goldschmidt M, Carvalho EM, Scott P. IL-17 mediates immunopathology in the absence of IL-10 following Leishmania major infection. PLoS Pathog. 2013; 9:e1003243. [PubMed: 23555256]

9. Novais FO, Carvalho LP, Graff JW, Beiting DP, Ruthel G, Roos DS, Betts MR, Goldschmidt MH, Wilson ME, de Oliveira CI, Scott P. Cytotoxic T cells mediate pathology and metastasis in cutaneous leishmaniasis. PLoS pathogens. 2013; 9:e1003504. [PubMed: 23874205]
10. Baluk P, Tammela T, Ator E, Lyubynska N, Achen MG, Hicklin DJ, Jeltsch M, Petrova TV, Pytowski B, Stacker SA, Yla-Herttuala S, Jackson DG, Alitalo K, McDonald DM. Pathogenesis of persistent lymphatic vessel hyperplasia in chronic airway inflammation. J. Clin. Invest. 2005; 115:247–257. [PubMed: 15668734]
11. Danese S, Sans M, Spencer DM, Beck I, Donate F, Plunkett ML, de la Motte C, Redline R, Shaw DE, Levine AD, Mazar AP, Fiocchi C. Angiogenesis blockade as a new therapeutic approach to experimental colitis. Gut. 2007; 56:855–862. [PubMed: 17170016]
12. Detmar M, Brown LF, Claffey KP, Yeo KT, Kocher O, Jackman RW, Berse B, Dvorak HF. Overexpression of vascular permeability factor/vascular endothelial growth factor and its receptors in psoriasis. J. Exp. Med. 1994; 180:1141–1146. [PubMed: 8064230]
13. Siafakas NM, Antoniou KM, Tzortzaki EG. Role of angiogenesis and vascular remodeling in chronic obstructive pulmonary disease. Int. J. Chron. Obstruct. Pulmon. Dis. 2007; 2:453–462. [PubMed: 18268919]
14. Chidlow JH Jr. Langston W, Greer JJ, Ostanin D, Abdelbaqi M, Houghton J, Senthilkumar A, Shukla D, Mazar AP, Grisham MB, Kevil CG. Differential angiogenic regulation of experimental colitis. Am. J. Pathol. 2006; 169:2014–2030. [PubMed: 17148665]
15. Huggenberger R, Siddiqui SS, Brander D, Ullmann S, Zimmermann K, Antsiferova M, Werner S, Alitalo K, Detmar M. An important role of lymphatic vessel activation in limiting acute inflammation. Blood. 2011; 117:4667–4678. [PubMed: 21364190]
16. Thomas SN, Rutkowski JM, Pasquier M, Kuan EL, Alitalo K, Randolph GJ, Swartz MA. Impaired humoral immunity and tolerance in K14-VEGFR-3-Ig mice that lack dermal lymphatic drainage. J. Immunol. 2012; 189:2181–2190. [PubMed: 22844119]
17. Ferrara N, Gerber HP, LeCouter J. The biology of VEGF and its receptors. Nat. Med. 2003; 9:669–676. [PubMed: 12778165]
18. Karkkainen MJ, Makinen T, Alitalo K. Lymphatic endothelium: a new frontier of metastasis research. Nat. Cell Biol. 2002; 4:E2–5. [PubMed: 11780131]
19. Huggenberger R, Ullmann S, Proulx ST, Pytowski B, Alitalo K, Detmar M. Stimulation of lymphangiogenesis via VEGFR-3 inhibits chronic skin inflammation. J. Exp. Med. 2010; 207:2255–2269. [PubMed: 20837699]
20. Cursiefen C, Chen L, Borges LP, Jackson D, Cao J, Radziejewski C, D'Amore PA, Dana MR, Wiegand SJ, Streilein JW. VEGF-A stimulates lymphangiogenesis and hemangiogenesis in inflammatory neovascularization via macrophage recruitment. J. Clin. Invest. 2004; 113:1040–1050. [PubMed: 15057311]
21. Halin C, Tobler NE, Vigl B, Brown LF, Detmar M. VEGF-A produced by chronically inflamed tissue induces lymphangiogenesis in draining lymph nodes. Blood. 2007; 110:3158–3167. [PubMed: 17625067]
22. Kataru RP, Jung K, Jang C, Yang H, Schwendener RA, Baik JE, Han SH, Alitalo K, Koh GY. Critical role of CD11b+ macrophages and VEGF in inflammatory lymphangiogenesis, antigen clearance, and inflammation resolution. Blood. 2009; 113:5650–5659. [PubMed: 19346498]
23. Nagy JA, Vasile E, Feng D, Sundberg C, Brown LF, Detmar MJ, Lawitts JA, Benjamin L, Tan X, Manseau EJ, Dvorak AM, Dvorak HF. Vascular permeability factor/vascular endothelial growth factor induces lymphangiogenesis as well as angiogenesis. J. Exp. Med. 2002; 196:1497–1506. [PubMed: 12461084]
24. Wuest TR, Carr DJ. VEGF-A expression by HSV-1-infected cells drives corneal lymphangiogenesis. J. Exp. Med. 2010; 207:101–115. [PubMed: 20026662]
25. Spath GF, Beverley SM. A lipophosphoglycan-independent method for isolation of infective Leishmania metacyclic promastigotes by density gradient centrifugation. Exp. Parasitol. 2001; 99:97–103. [PubMed: 11748963]
26. Gimblet C, Loesche MA, Carvalho L, Carvalho EM, Grice EA, Artis D, Scott P. IL-22 Protects against Tissue Damage during Cutaneous Leishmaniasis. PloS one. 2015; 10:e0134698. [PubMed: 26285207]

27. Titus RG, Marchand M, Boon T, Louis JA. A limiting dilution assay for quantifying Leishmania major in tissues of infected mice. Parasite Immunol. 1985; 7:545–555. [PubMed: 3877902]
28. Christian DA, Garbuzenko OB, Minko T, Discher DE. Polymer Vesicles with a Red Cell-like Surface Charge: Microvascular Imaging and in vivo Tracking with Near-Infrared Fluorescence. Macromol. Rapid Commun. 2010; 31:135–141. [PubMed: 21590885]
29. Weinkopff T, Mariotto A, Simon G, Hauyon-La Torre Y, Auderset F, Schuster S, Zangger H, Fasel N, Barral A, Tacchini-Cottier F. Role of Toll-like receptor 9 signaling in experimental Leishmania braziliensis infection. Infect. Immun. 2013; 81:1575–1584. [PubMed: 23439309]
30. Motoike T, Loughna S, Perens E, Roman BL, Liao W, Chau TC, Richardson CD, Kawate T, Kuno J, Weinstein BM, Stainier DY, Sato TN. Universal GFP reporter for the study of vascular development. Genesis. 2000; 28:75–81. [PubMed: 11064424]
31. Ahmed F, Pakunlu RI, Brannan A, Bates F, Minko T, Discher DE. Biodegradable polymersomes loaded with both paclitaxel and doxorubicin permeate and shrink tumors, inducing apoptosis in proportion to accumulated drug. J. Control Release. 2006; 116:150–158. [PubMed: 16942814]
32. Miles AA, Miles EM. Vascular reactions to histamine, histamine-liberator and leukotaxine in the skin of guinea-pigs. J. Physiol. 1952; 118:228–257. [PubMed: 13000707]
33. Ballet R, Emre Y, Jemelin S, Charmoy M, Tacchini-Cottier F, Imhof BA. Blocking junctional adhesion molecule C enhances dendritic cell migration and boosts the immune responses against Leishmania major. PLoS Pathog. 2014; 10:e1004550. [PubMed: 25474593]
34. Fraga CA, Oliveira MV, Alves LR, Viana AG, Sousa AA, Carvalho SF, De Paula AM, Botelho AC, Guimaraes AL. Immunohistochemical profile of HIF-1alpha, VEGF-A, VEGFR2 and MMP9 proteins in tegumentary leishmaniasis. An. Bras. Dermatol. 2012; 87:709–713. [PubMed: 23044562]
35. Mahnke A, Meier RJ, Schatz V, Hofmann J, Castiglione K, Schleicher U, Wolfbeis OS, Bogdan C, Jantsch J. Hypoxia in Leishmania major skin lesions impairs the NO-dependent leishmanicidal activity of macrophages. J. Invest. Dermatol. 2014; 134:2339–2346. [PubMed: 24583949]
36. Melby PC, Andrade-Narvaez FJ, Darnell BJ, Valencia-Pacheco G, Tryon VV, Palomo-Cetina A. Increased expression of proinflammatory cytokines in chronic lesions of human cutaneous leishmaniasis. Infect. Immun. 1994; 62:837–842. [PubMed: 8112853]
37. Singh AK, Mukhopadhyay C, Biswas S, Singh VK, Mukhopadhyay CK. Intracellular pathogen Leishmania donovani activates hypoxia inducible factor-1 by dual mechanism for survival advantage within macrophage. PloS one. 2012; 7:e38489. [PubMed: 22701652]
38. Becker I, Salaiza N, Aguirre M, Delgado J, Carrillo-Carrasco N, Kobeh LG, Ruiz A, Cervantes R, Torres AP, Cabrera N, Gonzalez A, Maldonado C, Isibasi A. Leishmania lipophosphoglycan (LPG) activates NK cells through toll-like receptor-2. Mol. Biochem. Parasitol. 2003; 130:65–74. [PubMed: 12946842]
39. Kropf P, Freudenberg MA, Modolell M, Price HP, Herath S, Antoniazi S, Galanos C, Smith DF, Muller I. Toll-like receptor 4 contributes to efficient control of infection with the protozoan parasite Leishmania major. Infect. Immun. 2004; 72:1920–1928. [PubMed: 15039311]
40. Schleicher U, Liese J, Knippertz I, Kurzmann C, Hesse A, Heit A, Fischer JA, Weiss S, Kalinke U, Kunz S, Bogdan C. NK cell activation in visceral leishmaniasis requires TLR9, myeloid DCs, and IL-12, but is independent of plasmacytoid DCs. J. Exp. Med. 2007; 204:893–906. [PubMed: 17389237]
41. Van Assche T, Deschacht M, da Luz RA, Maes L, Cos P. Leishmania-macrophage interactions: insights into the redox biology. Free Radic. Biol. Med. 2011; 51:337–351. [PubMed: 21620959]
42. Maruyama K, Asai J, Ii M, Thorne T, Losordo DW, D'Amore PA. Decreased macrophage number and activation lead to reduced lymphatic vessel formation and contribute to impaired diabetic wound healing. Am. J. Pathol. 2007; 170:1178–1191. [PubMed: 17392158]
43. Maruyama K, Ii M, Cursiefen C, Jackson DG, Keino H, Tomita M, Van Rooijen N, Takenaka H, D'Amore PA, Stein-Streilein J, Losordo DW, Streilein JW. Inflammation-induced lymphangiogenesis in the cornea arises from CD11b-positive macrophages. J. Clin. Invest. 2005; 115:2363–2372. [PubMed: 16138190]

44. Angeli V, Ginhoux F, Llodra J, Quemeneur L, Frenette PS, Skobe M, Jessberger R, Merad M, Randolph GJ. B cell-driven lymphangiogenesis in inflamed lymph nodes enhances dendritic cell mobilization. Immunity. 2006; 24:203–215. [PubMed: 16473832]
45. Goldman J, Rutkowski JM, Shields JD, Pasquier MC, Cui Y, Schmokel HG, Willey S, Hicklin DJ, Pytowski B, Swartz MA. Cooperative and redundant roles of VEGFR-2 and VEGFR-3 signaling in adult lymphangiogenesis. FASEB J. 2007; 21:1003–1012. [PubMed: 17210781]
46. Hong YK, Lange-Asschenfeldt B, Velasco P, Hirakawa S, Kunstfeld R, Brown LF, Bohlen P, Senger DR, Detmar M. VEGF-A promotes tissue repair-associated lymphatic vessel formation via VEGFR-2 and the alpha1beta1 and alpha2beta1 integrins. FASEB J. 2004; 18:1111–1113. [PubMed: 15132990]
47. Kunstfeld R, Hirakawa S, Hong YK, Schacht V, Lange-Asschenfeldt B, Velasco P, Lin C, Fiebiger E, Wei X, Wu Y, Hicklin D, Bohlen P, Detmar M. Induction of cutaneous delayed-type hypersensitivity reactions in VEGF-A transgenic mice results in chronic skin inflammation associated with persistent lymphatic hyperplasia. Blood. 2004; 104:1048–1057. [PubMed: 15100155]
48. Kajiya K, Hirakawa S, Detmar M. Vascular endothelial growth factor-A mediates ultraviolet B-induced impairment of lymphatic vessel function. Am. J. Pathol. 2006; 169:1496–1503. [PubMed: 17003502]
49. Zampell JC, Yan A, Avraham T, Daluvoy S, Weitman ES, Mehrara BJ. HIF-1alpha coordinates lymphangiogenesis during wound healing and in response to inflammation. FASEB J. 2012; 26:1027–1039. [PubMed: 22067482]
50. Felcht M, Luck R, Schering A, Seidel P, Srivastava K, Hu J, Bartol A, Kienast Y, Vettel C, Loos EK, Kutschera S, Bartels S, Appak S, Besemfelder E, Terhardt D, Chavakis E, Wieland T, Klein C, Thomas M, Uemura A, Goerdt S, Augustin HG. Angiopoietin-2 differentially regulates angiogenesis through TIE2 and integrin signaling. J. Clin. Invest. 2012; 122:1991–2005. [PubMed: 22585576]
51. Suri C, McClain J, Thurston G, McDonald DM, Zhou H, Oldmixon EH, Sato TN, Yancopoulos GD. Increased vascularization in mice overexpressing angiopoietin-1. Science. 1998; 282:468–471. [PubMed: 9774272]
52. Casanovas O, Hicklin DJ, Bergers G, Hanahan D. Drug resistance by evasion of antiangiogenic targeting of VEGF signaling in late-stage pancreatic islet tumors. Cancer cell. 2005; 8:299–309. [PubMed: 16226705]
53. Welti JC, Gourlaouen M, Powles T, Kudahetti SC, Wilson P, Berney DM, Reynolds AR. Fibroblast growth factor 2 regulates endothelial cell sensitivity to sunitinib. Oncogene. 2011; 30:1183–1193. [PubMed: 21057538]
54. Crawford Y, Kasman I, Yu L, Zhong C, Wu X, Modrusan Z, Kaminker J, Ferrara N. PDGF-C mediates the angiogenic and tumorigenic properties of fibroblasts associated with tumors refractory to anti-VEGF treatment. Cancer cell. 2009; 15:21–34. [PubMed: 19111878]
55. Erber R, Thurnher A, Katsen AD, Groth G, Kerger H, Hammes HP, Menger MD, Ullrich A, Vajkoczy P. Combined inhibition of VEGF and PDGF signaling enforces tumor vessel regression by interfering with pericyte-mediated endothelial cell survival mechanisms. FASEB J. 2004; 18:338–340. [PubMed: 14657001]
56. Chae SS, Kamoun WS, Farrar CT, Kirkpatrick ND, Niemeyer E, de Graaf AM, Sorensen AG, Munn LL, Jain RK, Fukumura D. Angiopoietin-2 interferes with anti-VEGFR2-induced vessel normalization and survival benefit in mice bearing gliomas. Clin. Cancer Res. 2010; 16:3618–3627. [PubMed: 20501615]
57. Osorio EY, Travi BL, da Cruz AM, Saldarriaga OA, Medina AA, Melby PC. Growth factor and Th2 cytokine signaling pathways converge at STAT6 to promote arginase expression in progressive experimental visceral leishmaniasis. PLoS Pathog. 2014; 10:e1004165. [PubMed: 24967908]
58. Xu G, Liu D, Fan Y, Yang X, Korner H, Fu YX, Uzonna JE. Lymphotoxin alpha beta 2 (membrane lymphotoxin) is critically important for resistance to Leishmania major infection in mice. J. Immunol. 2007; 179:5358–5366. [PubMed: 17911622]
59. Zhu M, Yang Y, Wang Y, Wang Z, Fu YX. LIGHT regulates inflamed draining lymph node hypertrophy. J. Immunol. 2011; 186:7156–7163. [PubMed: 21572030]

60. Okwor I, Xu G, Tang H, Liang Y, Fu YX, Uzonna JE. Deficiency of CD40 Reveals an Important Role for LIGHT in Anti-Leishmania Immunity. J. Immunol. 2015; 195:194–202. [PubMed: 26026056]

61. Browning JL, Allaire N, Ngam-Ek A, Notidis E, Hunt J, Perrin S, Fava RA. Lymphotoxin-beta receptor signaling is required for the homeostatic control of HEV differentiation and function. Immunity. 2005; 23:539–550. [PubMed: 16286021]

62. Tan KW, Yeo KP, Wong FH, Lim HY, Khoo KL, Abastado JP, Angeli V. Expansion of cortical and medullary sinuses restrains lymph node hypertrophy during prolonged inflammation. J. Immunol. 2012; 188:4065–4080. [PubMed: 22430738]

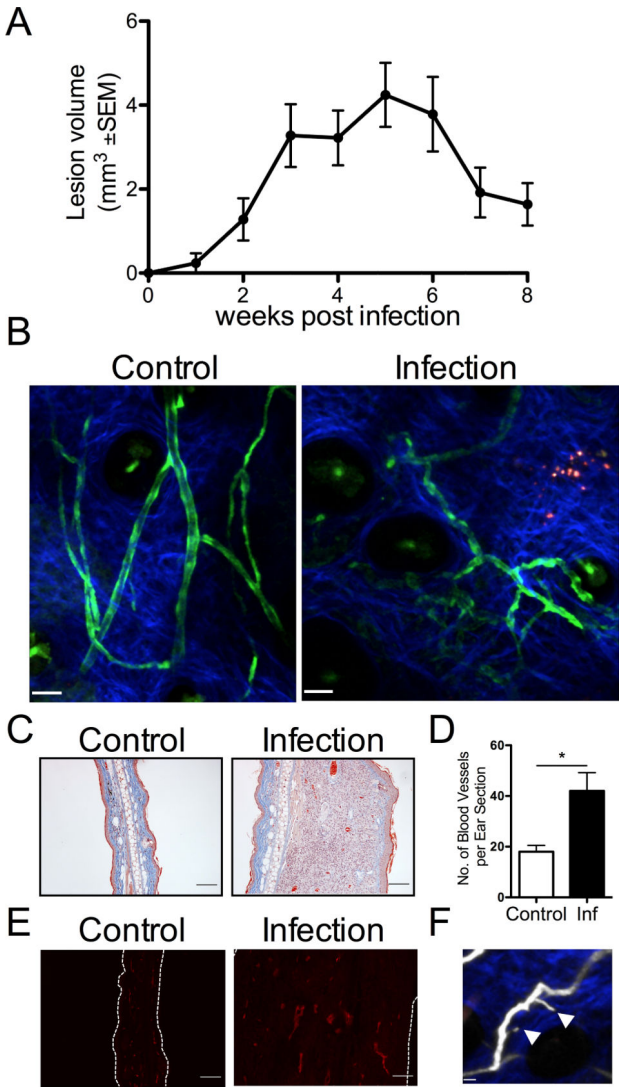

Fig. 1. Dermal vascular remodeling occurs during *L. major* infection

A: C57BL/6 mice were infected with 2×10^6 *L. major* metacyclic parasites in the ear dermis and lesion progression was monitored over time. **B:** Multiphoton microscopy of the dermis of Tie2-GFP-expressing mice infected for 5 wks compared to uninfected controls. **C:** Representative images of Masson's trichrome stain of infected and contralateral control ears from C57BL/6 mice showing vessels containing red blood cells. **D:** The total number of vessels per ear section quantified by microscopy at 5 wk p.i. with 3-5 mice per group. Data are shown as the mean +SEM and a *t*-test comparing infected mice to uninfected controls was performed. *P < 0.05. **E:** Confocal microscopy of frozen sections stained with antibodies against CD31 (red) showing alterations in the EC network with infection compared to naïve control C57BL/6 mice. **F:** EC sprouting is detected in infected mice (white arrowhead) after i.v. Evans blue to visualize the vasculature. Scale bars: (A) control 47 μm; infection 43 μm; (B and D) 100 μm; (E) 16 μm.

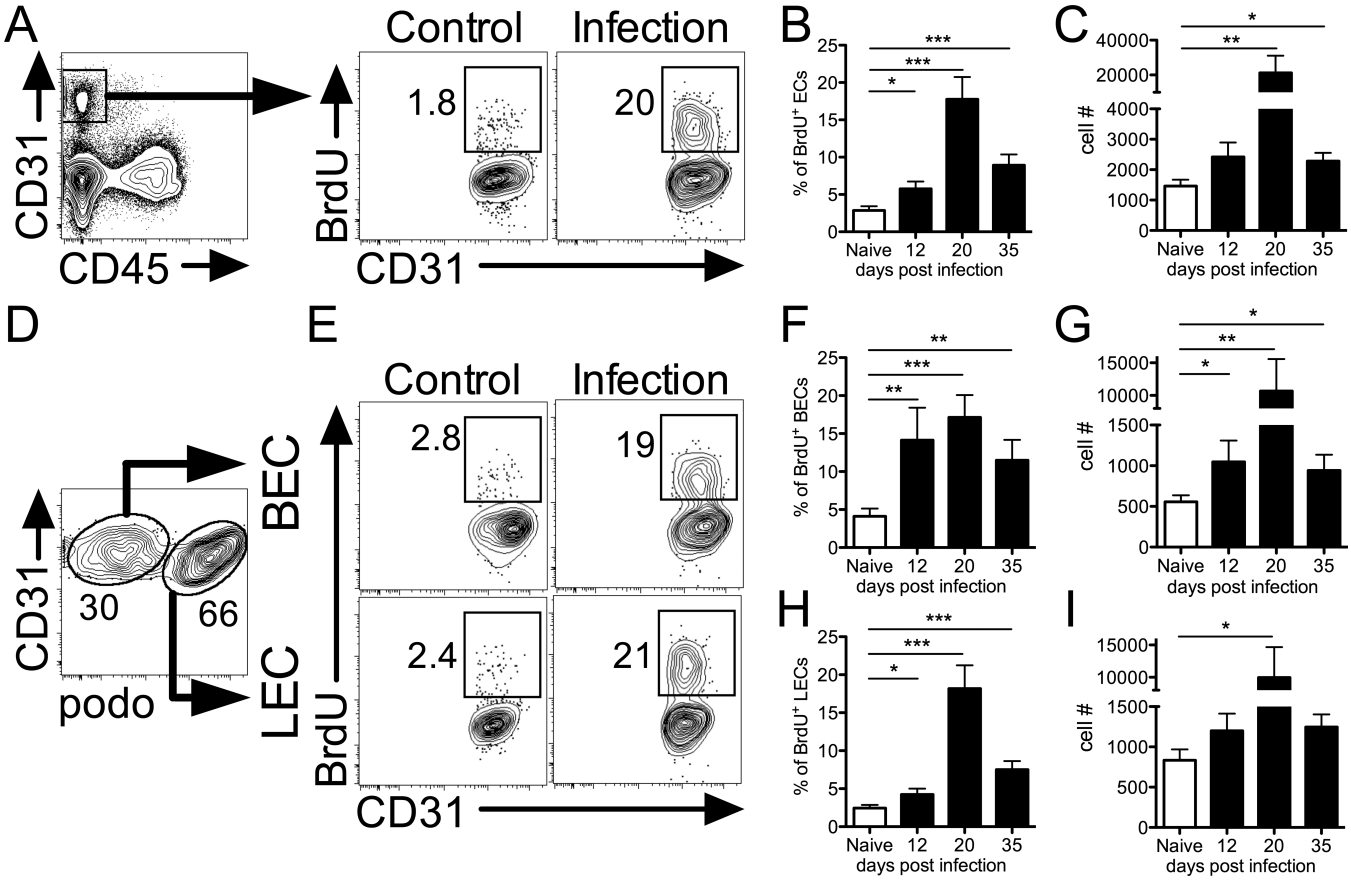

Fig. 2. Endothelial proliferation is detected at the site of infection during leishmaniasis

A: Representative flow cytometry plots showing gating of $CD31^+$ $CD45^-$ ECs and the percentage of ECs incorporating BrdU from naïve control and 20 d infected ears. Cells were gated on total, live, singlets previously. **B** and **C:** The percentage and number of proliferating $BrdU^+$ ECs in naïve ears and at 12, 20 and 35 d p.i. **D:** Dermal BEC and LECs were separated by podoplanin expression during FACS analysis. **E:** Representative flow plots showing the percentage of BECs and LECs incorporating BrdU from naïve and infected ears at 20 d p.i. **F** and **G:** Frequency and number of $BrdU^+$ BECs from naïve and infected ears at 12, 20 and 35 d p.i. **H** and **I:** Frequency and number of $BrdU^+$ LECs from naïve and infected ears at 12, 20 and 35 d p.i. Data is representative of at least one experiment depending on the time point with 4-5 mice per group per time point. Data are shown as the mean +SEM and a *t*-test comparing infected mice to naïve controls was performed. ***P < 0.0005, **P < 0.005, *P < 0.05.

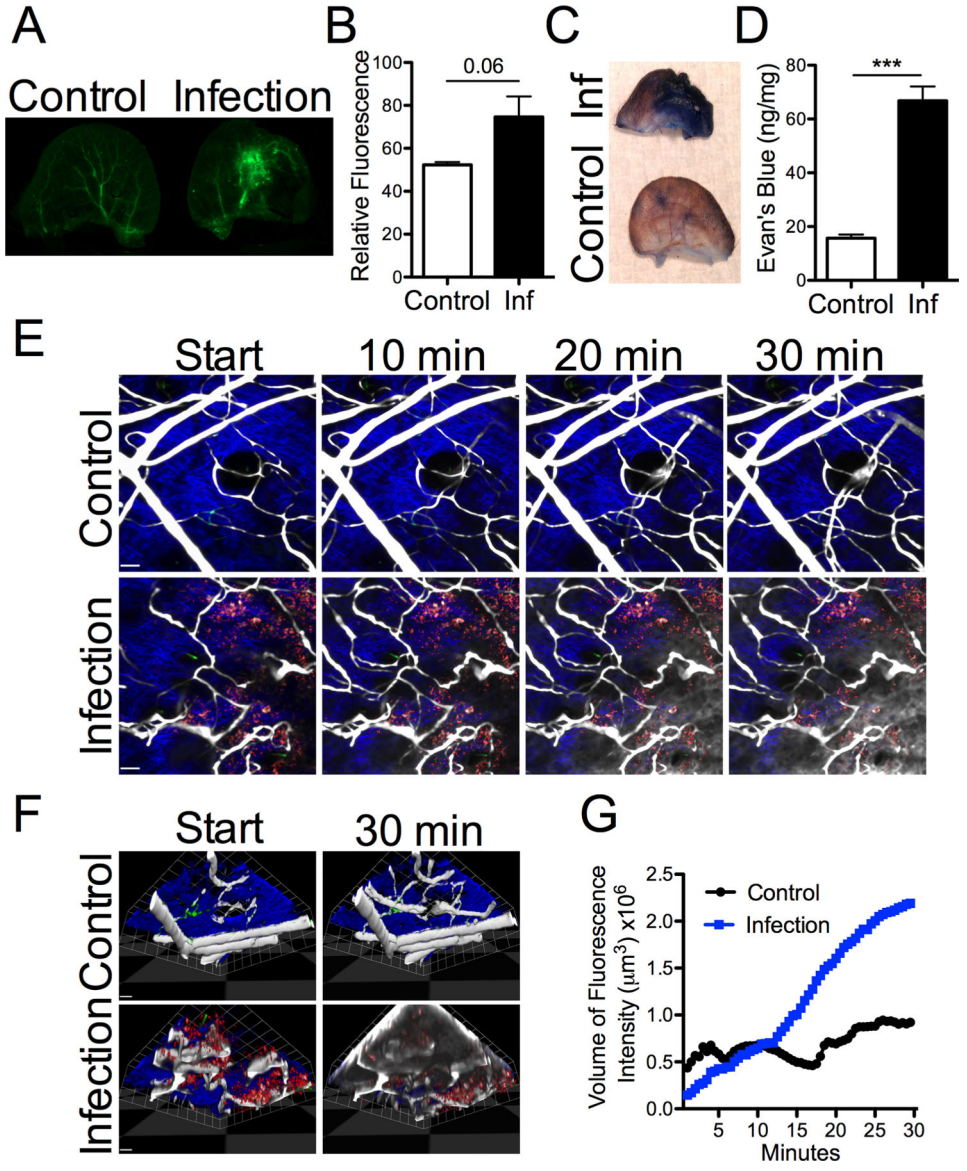

Fig. 3. Increased vascular permeability in the dermis is associated with *L. major* infection

C57BL/6 mice were infected with *L. major* parasites in the ear dermis and analyzed 5-6 wks p.i. **A:** Mice were injected i.v. with polymersomes containing near-infrared fluorophores and the accumulation of fluorescence was imaged from whole mount tissue sections of infected and control contralateral ears after 3 h. **B:** The total infrared fluorescence of each ear was quantified and data is representative of one experiment with 4 mice per group. **C** and **D:** Images of infected ears and naive controls 2 h after i.v. Evans blue with corresponding quantification from one representative experiment of two with 3-5 mice per group. **E-H:** Tie2-GFP-expressing mice were infected with DsRed-labeled *L. major* parasites i.d. and the dermis of infected and naïve mice was analyzed by multiphoton microscopy for 30 min. Time lapse 2D images **(E)** are shown every 10 min starting immediately after i.v. Evans blue. Sequential 3D images **(F)** are shown immediately after i.v. Evans blue and 30 min later. (Movies in Supp). Parasites are seen in red, Tie2 in green and Evans blue in white. **G:**

The quantification of the volume of fluorescence intensity of Evans blue in the extravascular space calculated every 30 s from the multiphoton imaging. Representative data from one infected and one control is shown with imaging data collected from at least 5 mice per group. Data are shown as the mean +SEM and a *t*-test comparing infected mice to controls was performed. ***P < 0.0005. Scale bar: (E) 45 μm; (F) 60 μm.

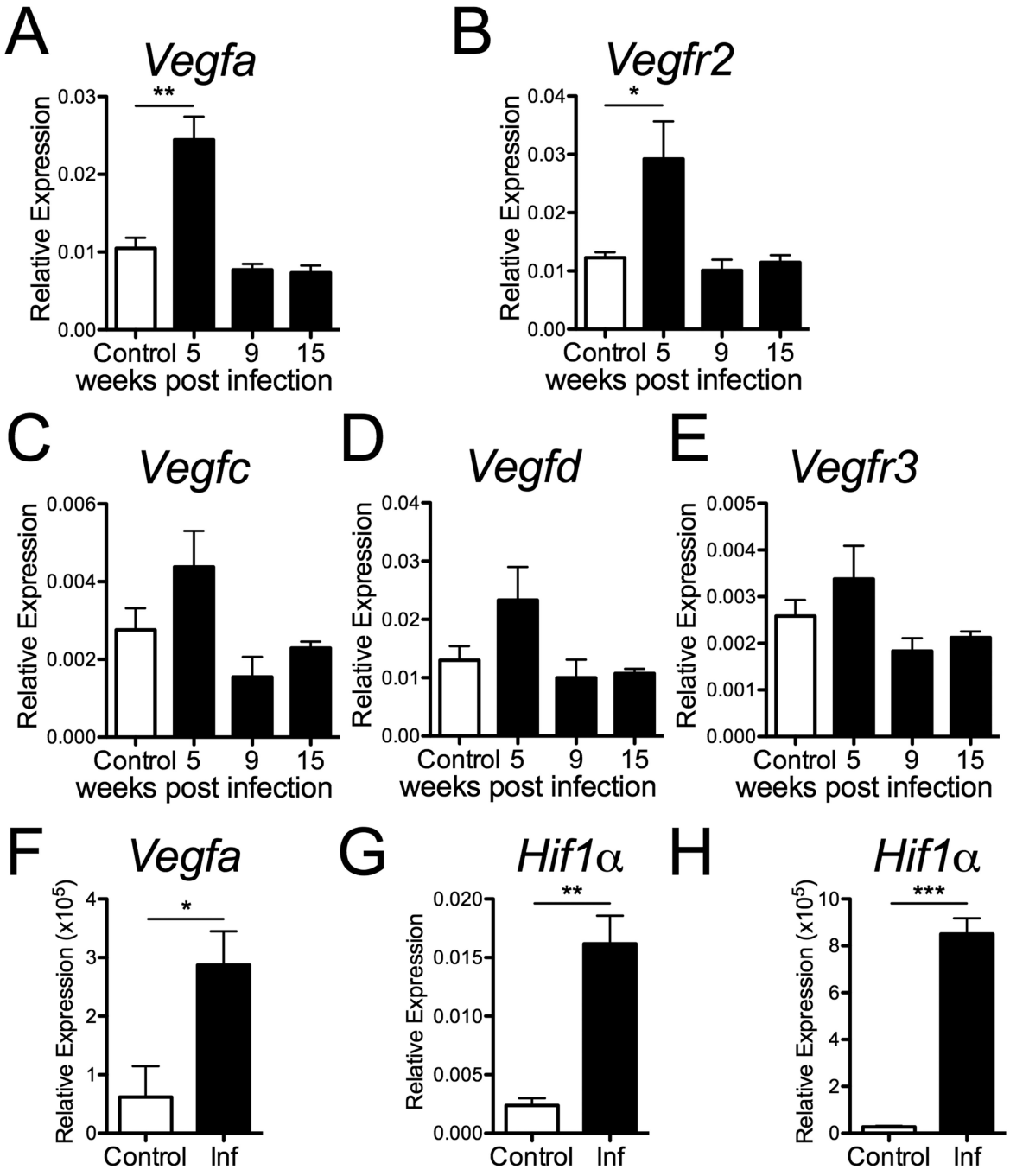

Fig. 4. VEGF-A and the corresponding receptor VEGFR-2 are expressed at increased levels at the site of *L. major* infection

C57BL/6 mice were infected with *L. major* parasites in the ear dermis and ears were analyzed by qRT-PCR at 5, 9 and 15 wks p.i. for the expression of VEGF-A **(A)**, VEGFR-2 **(B)**, VEGF-C **(C)**, VEGF-D **(D)**, and VEGFR-3 **(E)**. **F:** qRT-PCR for VEGF-A expression in LNs draining infected and naïve control ears at 5 wk p.i. **G and H:** qRT-PCR for HIF1α expression at 5 wk p.i. in naïve and infected ears **(G)** and dLNs **(H)**. Relative mRNA expression normalized to the housekeeping RPS11 gene is presented as the mean +SEM

with 5 mice per group. Data are representative of at least 2 independent experiments. ***P < 0.0005, **P < 0.005, *P < 0.05, *t*-test comparing infected mice to controls.

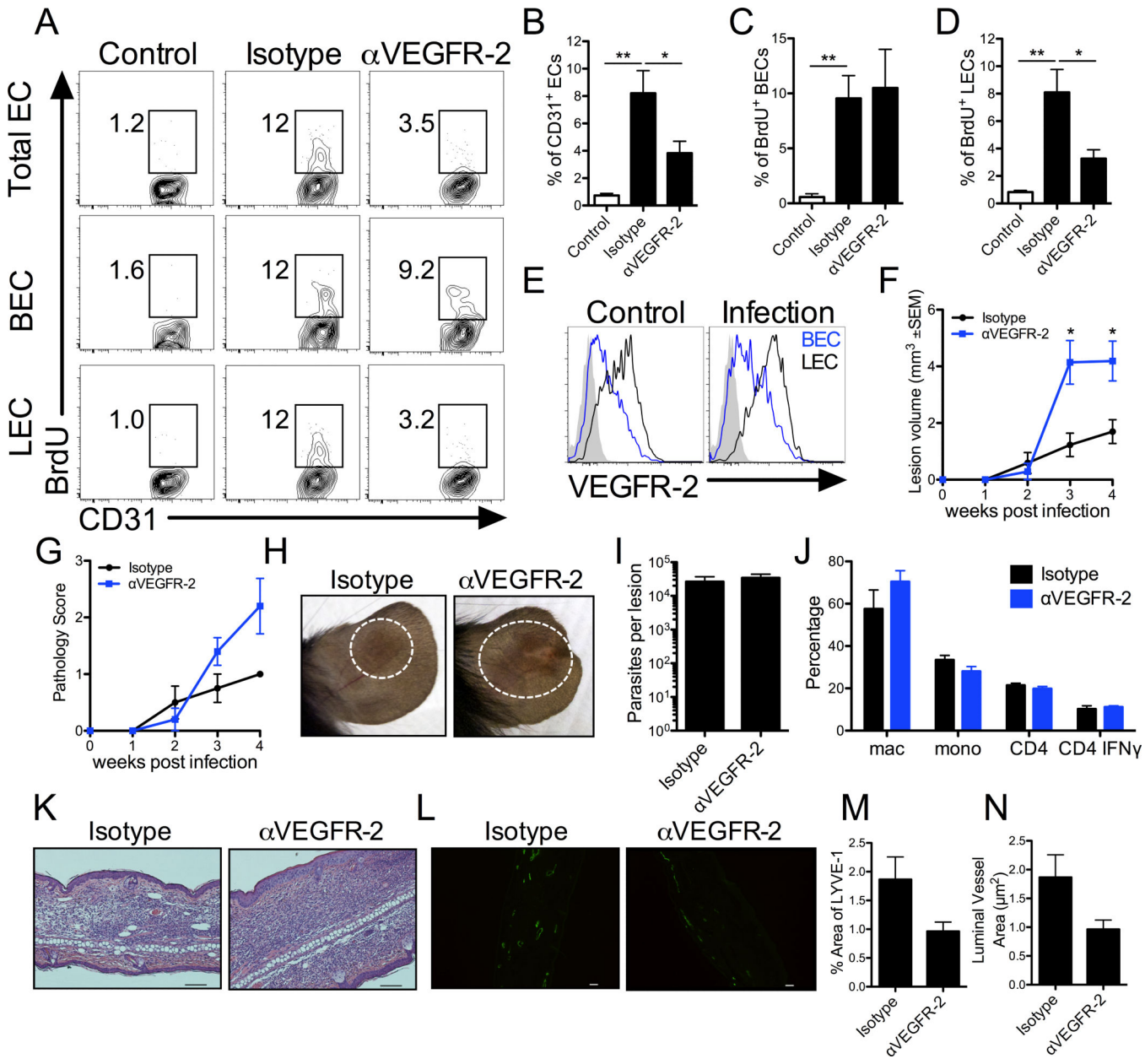

Fig. 5. VEGFR-2 blockade targets lymphatic endothelial cells and increases pathology during *L. major* infection

Mice were treated with αVEGFR-2 neutralization antibody or rat isotype control for the first 4 wks of infection. Naïve mice are shown as controls. **A:** Representative flow cytometry plots showing the percentage of $BrdU^+$ cells after gating on total, live, singlet, $CD31^+$ $CD45^-$ ECs and BECs ($CD31^+$ $podoplanin^-$) or LECs ($CD31^+$ $podoplanin^+$) individually. **B-D:** The quantification of the percentage of proliferating $BrdU^+$ cells of total ECs **(B)**, BECs **(C)** and LECs **(D)** from the skin of naïve controls or infected mice at 2 wks p.i. **E:** Representative flow cytometry histograms of BECs and LECs showing VEGFR-2 expression. **F:** Lesion volume was monitored over time. **G:** Lesion pathology was scored over time. **H:** Representative images of αVEGFR-2-treated and control ears at 4 wks p.i. **I:**

After 4 wks of αVEGFR-2 antibody treatment, the numbers of parasites in the ear were quantified by LDA. **J:** The quantification of the percentage of $CD64^+$ macrophages, and $Ly6C^+$ inflammatory monocytes of $CD11b^+$ cells, and $CD4^+$ T cells of $CD45^+$ cells in the skin after gating on total, live, singlets from αVEGFR-2 treated or control animals at 4 wks p.i. was assessed by flow cytometry. The quantification of the percentage of $CD4^+$ T cells from the dLN producing IFNγ was assessed by flow cytometry after ex vivo treatment with PMA and ionomycin in the presence of BFA for 4 hours. **K:** Representative H and E stained ear sections of αVEGFR-2-treated and control ears at 4 wks p.i. **L:** Confocal microscopy of frozen sections stained for LYVE-1 (green) at 4 wks p.i. from αVEGFR-2-treated and control animals. **M-N:** Quantification of the density and luminal area of $LYVE\text{-}1^+$ vessels. Data are representative of at least 2 independent experiments with 4-5 mice per group. Data are shown as the mean ±SEM and a *t*-test comparing mice receiving αVEGFR-2 Ab to isotype controls was performed. $^{**}P < 0.005$, $^{*}P < 0.05$. Scale bar: 100 μm.